Demonstration of multitarget wireless sensing using high-scanning-rate coupled-patch antenna

Shuguang Xiao, Zhaoxin Chang, Jiachen Du, Ge Zhang, Amir Rashid, Yi Huang, Chaijie Duan, Daqing Zhang, Qingfeng Zhang

Demonstration of Multi-Target Wireless Sensing Using High-Scanning-Rate Coupled-Patch Antenna

Shuguang Xiao, Zhaoxin Chang, Jiachen Du, Ge Zhang, Amir K. Rashid, Yi Huang, Chaijie Duan, Daqing Zhang, *Fellow, IEEE*, and Qingfeng Zhang, *Senior Member, IEEE*

***Abstract*—This paper proposes a frequency-diverse multi-target wireless sensing system for integrated sensing and communication (ISAC) applications. A coupled-patch antenna (CPA) with frequency-dependent beam scanning capability is employed as the key component for multi-target localization and respiration detection. Owing to the high scanning rate of 25.8° per 1% bandwidth, the designed CPA is able to continuously scan an angle range of 93° across broadside as frequency varies from 3.26 GHz to 3.38 GHz, which well fits the ISAC application in Sub-6 GHz frequency. Four examples are given to demonstrate the benefit of high-scanning-rate CPA for multi-target localization, respiration detection, and surrounding interference mitigation.**

***Index Terms*—Frequency diverse, high scanning rate, coupled-patch antenna, multi-target sensing, respiration detection.**

I. Introduction

The integration of sensing and communication (ISAC) holds great promise as a cutting-edge research domain, envisioned to revolutionize future communication systems with their dual capabilities in information exchange and sensing functionality [1], [2]. The ingenious integration of wireless sensing within the confines of a robust communication infrastructure has emerged as a pivotal part of ISAC.

In the complex tapestry of a multi-target wireless sensing environment, where the propensity for mutual occlusion is rife, the ability to discern individual targets hinges upon the acuity of the angular resolution in delineating their respective vistas. This, in turn, is intricately interwoven with the capacity for interference mitigation, ensuring that each target's visibility is not obscured by others [3]. Conventional multi-target sensing solutions mainly include AOA estimation scheme [4], [5] and digital beamforming scheme [6]. However, these signal processing algorithms [7] ultimately rely on the utilization of multiple antennas at the expense of bulky, expensive and complex electronic systems [8]. Recently, microwave imaging and sensing using frequency scanning antenna (FSA) has been proposed [9], [10]. It features simple and low-cost architecture owing to its beam scanning capability based on a single leaky-wave antenna. However, the leaky-wave antennas used in [9], [10] have relatively low scanning rates, which are defined as the ratio of scan range to relative bandwidth. As a result, their significant utilization of extensive spectrum resources for beam scanning, coupled with the need for high sampling rates in analog-to-digital (A/D) converters in baseband systems, renders them unsuitable for integration into ISAC application. Various techniques have been proposed to enhance the scanning rate of FSA [11]–[22]. Among these, coupled waveguide resonator antenna [21] and coupled-patch arrays (CPAs) [22] with extremely high scanning rate are the most promising candidates for ISAC. However, the coupled waveguide resonator antenna [21] is bulky and CPAs in [22] has limited scanning range of 37° in the forward quadrant only. Therefore, low-profile planar FSAs with extremely high scanning rate and wide scanning range is highly desired and their applications to multi-target sensing need to be demonstrated.

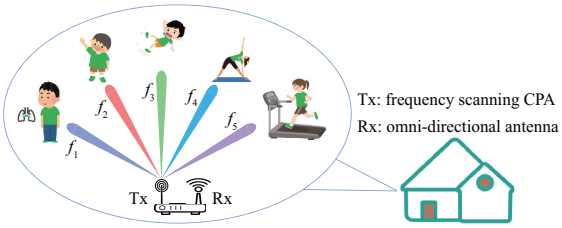

Fig. 1: Proposed multi-target sensing architecture using frequency-diverse CPA.

In this letter, we demonstrate a frequency-diverse multi-target sensing system based on a wide-angle and high scanning-rate CPA for ISAC. The designed CPA is able to continuously scan an angle range of 93° in both forward and backward quadrants as frequency varies from 3.26 GHz to 3.38 GHz within the frequency band of Sub-6 GHz wireless communication. Four application examples are provided to show the benefits of wide-angle and high scanning-rate CPA for multi-target sensing.

II. Principle

A. Wireless Sensing Using Frequency-Diverse CPA

Fig. 1 shows the architecture of the proposed frequency-diverse multi-target wireless sensing system, where a wide-

Manuscript received 2024. This work is supported partly by the Basic and Applied Basic Research Foundation of Guangdong Province (2021B1515120029), partly by the Shenzhen Key Laboratory of EM Information (ZDSYS20210709113201005), partly by the High-Level Special Funds (G03034K004), and partly by the Major Key Project of PCL2023AS1-3. *(S. Xiao and Z. Chang contributed equally to this work.) (Corresponding Authors: Qingfeng Zhang; Daqing Zhang)*

S. Xiao, J. Du, A. Rashid, and Q. Zhang are with State Key Laboratory of Optical Fiber and Cable Manufacture Technology, Department of Electronic and Electrical Engineering, Southern University of Science and Technology, and with the National Center for Applied Mathematics Shenzhen, Shenzhen, 518055, China. S. Xiao is also with G. Zhang at Peng Cheng Laboratory, China. Z. Chang is with SAMOVAR, Telecom SudParis, Institut Polytechnique de Paris, Palaiseau 91120, France. J. Du is also with City University of Hong Kong. Y. Huang and C. Duan are with Shenzhen HUAYI Medical Technologies Co., Ltd, Shenzhen, Guangdong, China. D. Zhang is with the School of Computer Science, Peking University, Beijing 100871, China, and also with SAMOVAR, Telecom SudParis, Institut Polytechnique de Paris, Palaiseau 91120, France. (Email: zhang.qf@sustech.edu.cn; daqing.zhang@telecom-sudparis.eu)

angle and high scanning-rate CPA serves as the transmitter and an omni-directional antenna is employed as the receiver. In a nutshell, we replace the transmitting antenna in the traditional wireless communication system with a wide-angle and high scanning-rate CPA. Since signals of different frequencies are transmitted to different angles by CPA, by analyzing the signal of each frequency component, information from different angles can be identified. Therefore, by using frequency-diverse CPA, such a single input single output (SISO) wireless system enables beam scanning capability which is usually achieved by expensive multiple input multiple output (MIMO) technology in traditional wireless sensing system [23]–[26]. So the proposed method provides a simple and low-cost system architecture for wireless sensing.

Although wireless sensing has demonstrated promising performance in many applications, it still faces one fundamental challenge, that is, low capability to distinguish multiple targets and/or interfering objects. When there are multiple targets and/or interfering objects in the environment, the reflection signals from these objects are superimposed at the receiver. Therefore, how to separate each target signal from the received signal becomes a key challenge. The proposed frequency-diverse wireless sensing system, incorporating CPA as the key feature, exhibits significant advantages in distinguishing multiple targets compared to conventional SISO wireless systems utilizing all omnidirectional antennas. To better show these benefits, let us now consider respiration detection of human body as the application scenario. In this case, the interference may come from strong Line-of-Sight (LoS) static path from environment, other moving targets, and self movement. The impact of interference on received signals can be characterized using the channel state information (CSI), which contains both target and interference information [27]–[29]. Denote the transmitted signal as $s(t)$, the received signal is the convolution of the CSI and the transmitted signal, $y(t) = H(f,t) * s(t)$. Mathematically, CSI is expressed by

$$H(f,t) = \sum_{n=1}^{N} A_n(f,t) e^{-jk_0 d_n(t)}, \tag{1}$$

where N is the number of reflecting paths contributed by both target and interference, k_0 is wave number at frequency f, $A_n(f,t)$ is the reflection amplitude of the n-th path, and $d_n(t)$ is the length of the n-th reflection path. The sum of all the paths in (1) can be divided into two parts, $H(f,t) = H_{\text{int}}(f,t) + H_{\text{tar}}(f,t)$, where $H_{\text{tar}}(f,t)$ denotes the contribution by the target that we want to detect, and $H_{\text{int}}(f,t)$ denotes the rest contribution from interference. So the CSI in (1) can be reformulated as

$$H(f,t) = H_{\text{int}}(f,t) + A_{\text{tar}}(f,t) e^{-jk_0 d_{\text{tar}}(t)}, \tag{2}$$

where $A_{\text{tar}}(f,t)$ and $d_{\text{tar}}(t)$ are the complex attenuation and length of the target path $H_{\text{tar}}(f,t)$.

In some special cases where there is only static interference, it is easy to distinguish $H_{\text{tar}}(f,t)$ from $H_{\text{int}}(f,t)$ by using pure signal processing. Let us use $H_s = H_{\text{int}}(f,t)$ to denote this static interference. As shown in Fig. 2, the CSI can be represented as the addition of two vectors on the complex plane.

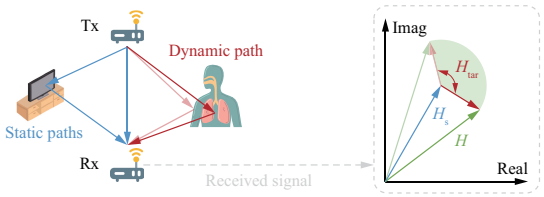

Fig. 2: Illustration of CSI on the complex plane.

The static vector is the sum of all static object-reflected signals, which is constant. The dynamic vector corresponding to the target-reflected signal rotates with respect to the static vector as respiration is going on. As the target inhales and exhales during respiration, the dynamic reflection path length increases and decreases accordingly. Thus, the dynamic vector rotates on the complex plane and the phase change is determined by the displacement of respiration [30]. In this static interference case, the constant static vector H_s can be approximated as the center of dynamic vector and hence can be easily removed by pure signal processing [31].

In the cases where the interference comes from moving objects, e.g. a person walking around or the respiration from another person, the interference vector $H_{\text{int}}(f,t)$ will be complicated and pure signal processing is almost impossible if no prior information about the interference is available. This has become the most challenging problem in wireless sensing [32]. The proposed frequency-diverse sensing system using CPA provides a new perspective to look into this problem from the physical layer. CPA transmits different frequencies to different directions, which naturally divides physical channels through angle-frequency correspondence. Therefore, one is able to remove interference from unwanted angles through frequency selection. We will design four sensing examples to illustrate this in Sec. III.

B. Design of Wide-Angle and High Scanning-Rate CPA

We design a wide-angle and high-scanning-rate CPA for this sensing system. Fig. 3 shows the configuration of CPA and the corresponding circuit model. It consists of twelve patch resonators which couple with each other through alternating iris windows and gaps. The iris is formed by using via hole array in the middle of patch and a window is left for wave coupling. Such iris windows are equivalent to magnetic couplers, which are denoted as $J_{12}, J_{34}, \ldots, J_{11,12}$ in Fig. 3(b). The coupling gaps are equivalent to electric couplers, which are denoted as $J_{23}, \ldots, J_{10,11}$ in Fig. 3(b). The employment of alternating magnetic and electric couplings is the key to realize continuous beam scanning across broadside, which has been well explained in [21]. The designed CPA is modeled by a coupled-resonator network in Fig. 3(b). One employs a coupling matrix, M, to describe all the coupling values between resonators. The reflection coefficient at the port, S_{11}, can be calculated using M by

$$S_{11}(\omega) = 1 + 2[jM + j\omega I + R]^{-1}_{1,1}, \tag{3}$$

where I is an identity matrix and R has zeros in all the entries except for (1,1) being one. By using (3), one is able to

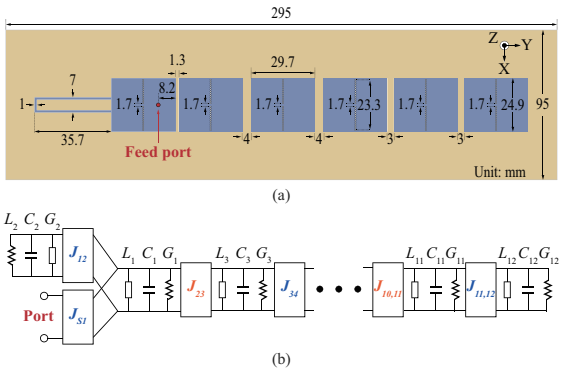

Fig. 3: (a) Configuration and (b) equivalent circuit of the designed CPA.

synthesize and tune the reflection response. In summary, the high-quality resonators featuring sharp phase change within a narrow frequency band provide an extremely high scanning rate for CPA [21], and the coupling matrix theory in filters [33] provide a good tool to tune the desired response.

The proposed CPA is designed on a double-layer printed circuit board (PCB). It employs a 0.787 mm thick substrate, with dielectric constant and loss tangent of 2.2 and 0.0009, respectively. Fig. 4(a) shows the photograph of fabricated prototype and the measured reflection response. Note that the reflection is below -10 dB within the operational frequency band $3.23-3.38$ GHz for wireless sensing. Although the designed CPA is able to work in an even wider frequency band, the selected band $3.26-3.38$ GHz is good enough for experimental demonstration of multi-target sensing in Sub-6 GHz indoor wireless communication band. Fig. 4(b) shows the measured beam angles and realized gains within $3.26-3.38$ GHz. The beam continuously scans from $-55°$ to $38°$ within $3.26-3.38$ GHz, which is equivalent to a scanning rate of $25.8°$ per 1% bandwidth. This design has a much wider scanning range ($93°$) and higher scanning rate than other reported CPAs, e.g. [22]. The measured average gain is about 5.8 dBi within the operational frequency band.

In summary, we designed a wide-angle and high scanning-rate CPA for experimental demonstration of multi-target wireless sensing within the operational frequency band $3.26-3.38$ GHz. It scans an angle range of $93°$ and exhibits a high scanning rate of $25.8°$ per 1%. The system demonstration based on the designed CPA will be introduced in the forthcoming section.

III. System Demonstration of Wireless Sensing

For experimental demonstration of the proposed wireless sensing system in Fig. 1, we employ the designed CPA in Fig. 3(a) as the transmitting antenna and use an omnidirectional antenna as the receiving antenna. For proof of concept, we use a Keysight N5227A vector network analyzer (VNA) to serve as the transceiver, which sends signals within the operational frequency band at a step of 10 MHz. The ground truth value of respiration rate is collected through a NUL-236 belt [34]. Four different cases are given to demonstrate the benefits of proposed wireless sensing system based on CPA.

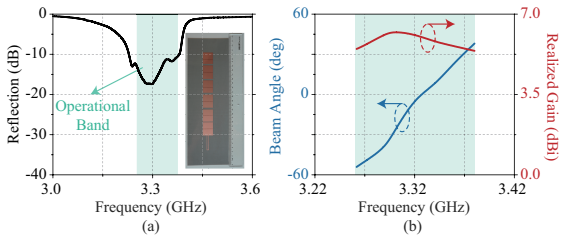

Fig. 4: Measured responses of the designed CPA: (a) reflection response; (b) beam angle and realized gain versus frequency.

A. Case I: Single-Target Localization Using Respiration Detection

In the first case, we demonstrate the localization of a single target according to respiration detection. As shown in Fig. 5 (a), we let a single target sit at four different locations corresponding to four angles with respect to the transmitting CPA. The principle for localization of the target is that the received signal at the frequency corresponding to the user's angle should show obvious signal fluctuations caused by respiration. Meanwhile, the fluctuations at other frequencies are not obvious because the signals at these frequencies are sent to angles where the target does not exist.

Based on the above principle, we introduce the procedure of estimating the angle of the target as follows. Firstly, we use VNA to collect the transmission parameters (S_{21}) at various frequencies corresponding to different transmission angles. The sampling rate of data is 13 Hz, corresponding to collecting once after every 77 ms. So we have a time series of complex signals for each frequency. We subsequently perform the Fast Fourier Transform (FFT) for the complex signals of each frequency. Since the signal fluctuation is caused by periodic respiration, the spectrum after FFT shows an energy peak at the respiration rate. We sum up the energy within the respiration frequency band (0.1 Hz - 0.4 Hz) as the breath energy (BE). Then, we compute the BEs at different frequencies and locate the frequency of maximum BE. Finally, we convert the frequency to angle according to Fig. 4(b).

In Fig. 5 (a), we let the target sit at -50°, -25°, 0°, and 25°, respectively. The corresponding BEs across all frequencies of each location are shown in Fig. 5(b). It can be seen that the peak value of BE appears at 3.27 GHz, 3.3 GHz, 3.33 GHz, and 3.36 GHz, aligning with the angle of the target according to Fig. 4(b). In summary, the proposed frequency-diverse wireless sensing system based on CPA is able to accurately identify a single target sitting at different locations through respiration detection.

B. Case II: Multi-Target Localization using Respiration

In the second case, we demonstrate the simultaneous localization of multiple targets according to respiration detection. As shown in Fig. 6 (a), three targets sit side by side in front of CPA. The left two targets are separated by 30 cm, while the right two targets are only 10 cm apart. We utilize a similar signal processing scheme as the Case I. As shown in Fig. 6 (b), the peak values of BE appear at 3.29 GHz, 3.33 GHz, and 3.36 GHz respectively. These three frequencies correspond to

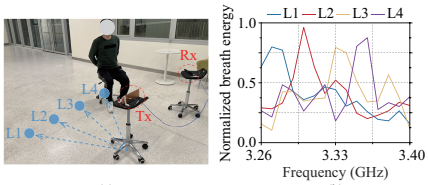

(a) (b)

Fig. 5: Localization of a single target at different locations: (a) experiment setup; (b) breath energies (BEs) versus frequency at different locations (L1, L2, L3, and L4).

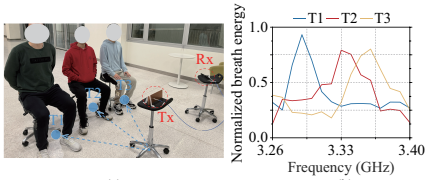

(a) (b)

Fig. 6: Simultaneous localization of multiple targets at different locations: (a) experiment setup; (b) BEs of different targets (T1, T2, and T3).

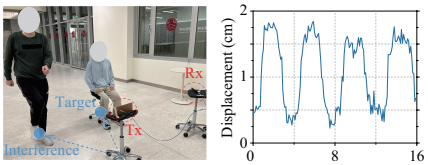

(a) (b)

Fig. 7: Mitigating interference from a moving person: (a) experiment setup; (b) extracted respiration signal.

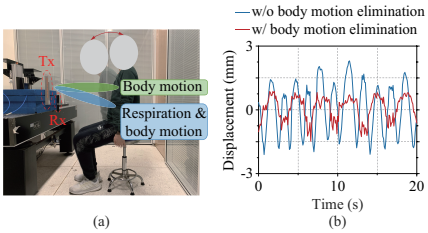

(a) (b)

Fig. 8: Eliminating self-body motion interference for respiration monitoring: (a) experiment setup; (b) extracted respiration signals before and after motion elimination.

-40°, 0°, and 24°, respectively, which are consistent with the targets' locations. One should note that if some targets exhibit the same respiration rate in this case, it is still possible to identify them using advanced signal processing algorithm [35]. In summary, we successfully demonstrate the capability of the proposed system for multi-target sensing.

C. Case III: Mitigating Interference from Moving Person

In the third case, we consider a more challenging application scenario where the target is interfered by a moving person. Since the movement scale of the interfering person (e.g., walking) may be larger than respiration of the target person, separating the respiration signal from the interference signal poses a significant challenge for conventional wireless sensing systems. As shown in Fig. 7 (a), the sensing target is breathing normally while the interfering object is walking near the target with 1 m distance away. We calculate the BE for each frequency corresponding to each transmitting beam of CPA. The angle with the highest BE is identified as the angle of target. We further extract the respiration waveform using the signal of this frequency aligning with the angle of target. As shown in Fig. 7 (b), despite the interference from moving person nearby, the target's respiration waveform can still be observed clearly. In summary, we demonstrate that the proposed wireless sensing system is able to mitigate interference from a moving person in the environment.

D. Case IV: Mitigating Interference from Self-Body Motion

In the fourth case, we demonstrate that the proposed sensing system achieves fine-grained respiration monitoring under self-body motion interference. Currently, most sensing systems require the target to stay static during the sensing process. If the body is also in motion, the fluctuations of these movements mix with the fluctuations induced by respiration. It is hard to extract the respiration from the received signal because the body motion has a larger scale [36]. Here we demonstrate that CPA is able to solve this issue. The key idea is that the body area near the target area (i.e., chest for respiration monitoring) exhibits the same body motion as the target area, but no target motion (i.e., respiration). So one transmits two beams to these two areas by controlling frequency of CPA and subsequently subtracts the reflected signals from these two areas. This will eliminate the body motion while retaining the target motion. As shown in Fig. 8 (a), the transmitting antenna is placed along the vertical direction so that signals of different frequencies are sent to different parts of the human body. The person shakes his body back and forth in front of the antennas. We extracted the reflected signal of the abdomen (3.31 GHz, corresponding to -24°) and the reflected signal of the chest (3.33 GHz, corresponding to 0°) respectively. As shown in Fig. 8 (b), raw abdomen displacement is dominated by large-scale and high-frequency body shake. After body motion elimination, the displacement of abdomen is consistent with the periodic fluctuations caused by respiration. In summary, the proposed sensing system can eliminate body motion in respiration monitoring.

One should note that all the above experiments are conducted in a relatively open environment, where light-of-sight paths are the main contributions. In the real-world applications, multiple path may slightly complicate the signal processing. Moreover, the quality of transceivers also affect the signal-to-noise ratio and may bring in errors to the sensing result. We will explore these in future research.

IV. CONCLUSIONS

We have demonstrated a frequency-diverse multi-target wireless sensing system based on wide-angle and high scanning-rate CPA for ISAC applications. Four examples were given to demonstrate the benefit of high-scanning-rate CPA for multi-target localization, respiration detection, and surrounding interference mitigation. Although the proposed CPA is not suitable for light-of-sight point-to-point communication, it is still applicable for wireless indoor communication where rich scattering exists. In future research, we will further enhance scanning range and gain of CPA, and explore optimal balance between sensing and communication in ISAC application.

REFERENCES

[1] F. Liu, Y. Cui, C. Masouros, J. Xu, T. X. Han, Y. C. Eldar, and S. Buzzi, "Integrated sensing and communications: Toward dual-functional wireless networks for 6G and beyond," *IEEE J. Sel. Areas Commun.*, vol. 40, no. 6, pp. 1728–1767, Jun. 2022.

[2] D. Zhang, D. Wu, K. Niu, X. Wang, F. Zhang, J. Yao, D. Jiang, and F. Qin, "Practical issues and challenges in CSI-based integrated sensing and communication," in *Proc. IEEE Int. Conf. Commun. Workshops (ICC Workshops)*. IEEE, May 2022, pp. 836–841.

[3] M. I. Skolnik, *Introduction to Radar Systems, 3rd Edition*. McGraw-Hill, 2001.

[4] Q. Gao, J. Tong, J. Wang, Z. Ran, and M. Pan, "Device-free multi-person respiration monitoring using WiFi," *IEEE Trans. Veh. Technol.*, vol. 69, no. 11, pp. 14 083–14 087, Nov. 2020.

[5] X. Li, S. Li, D. Zhang, J. Xiong, Y. Wang, and H. Mei, "Dynamic-MUSIC: Accurate device-free indoor localization," in *Proc. ACM Int. Joint Conf. Pervasive Ubiquitous Comput. (Ubicomp)*, 2016, pp. 196–207.

[6] J. Xiong, H. Hong, H. Zhang, N. Wang, H. Chu, and X. Zhu, "Multi-target respiration detection with adaptive digital beamforming technique based on SIMO radar," *IEEE Trans. Microw. Theory Techn.*, vol. 68, no. 11, pp. 4814–4824, Nov. 2020.

[7] Y. Li, D. Wu, J. Zhang, X. Xu, Y. Xie, T. Gu, and D. Zhang, "DiverSense: Maximizing Wi-Fi sensing range leveraging signal diversity," *Proc. ACM Interact. Mob. Wearable Ubiquitious Technol.*, vol. 6, no. 2, pp. 1–28, 2022.

[8] L. Guan, Z. Zhang, X. Yang, N. Zhao, D. Fan, M. A. Imran, and Q. H. Abbasi, "Multi-person breathing detection with switching antenna array based on WiFi signal," *IEEE J. Transl. Eng. Health Med.*, vol. 11, pp. 23–31, 2023.

[9] D. Ma, J. Zhong, S. Shen, A. Dubey, C. Zhang, Q. Zhang, and R. Murch, "Single-shot frequency-diverse near-field imaging using high-scanning-rate leaky-wave antenna," *IEEE Trans. Microw. Theory Techn.*, vol. 69, no. 7, pp. 3399–3412, Jul. 2021.

[10] Y. Yuan, C. Lu, A. Y.-K. Chen, C.-H. Tseng, and C.-T. M. Wu, "Multi-target concurrent vital sign and location detection using metamaterial-integrated self-injection-locked quadrature radar sensor," *IEEE Trans. Microw. Theory Techn.*, vol. 67, no. 12, pp. 5429–5437, Dec. 2019.

[11] J. Chen and Q. Zhang, "High scanning-rate periodic leak-wave antennas using complementary microstrip-slotline stubs," *Proc. 6th Asia-Pacific Conf. Antennas Propag.*, pp. 1–3, Oct. 2017.

[12] D.-F. Guan, P. You, Q. Zhang, Z.-H. Lu, S.-W. Yong, and K. Xiao, "A wide-angle and circularly polarized beam-scanning antenna based on microstrip spoof surface plasmon polariton transmission line," *IEEE Antennas Wireless Propag. Lett.*, vol. 16, pp. 2538–2541, 2017.

[13] Q. Zhang, Q. Zhang, and Y. Chen, "Spoof surface plasmon polariton leaky-wave antennas using periodically loaded patches above PEC and AMC ground planes," *IEEE Antennas Wireless Propag. Lett.*, vol. 16, pp. 3014–3017, 2017.

[14] G. Zhang, Q. Zhang, S. Ge, Y. Chen, and R. D. Murch, "High scanning-rate leaky-wave antenna using complementary microstrip-slot stubs," *IEEE Trans. Antennas Propag.*, vol. 67, no. 5, pp. 2913–2922, May 2019.

[15] S. Ge, Q. Zhang, C.-Y. Chiu, Y. Chen, and R. D. Murch, "Single-side-scanning surface waveguide leaky-wave antenna using spoof surface plasmon excitation," *IEEE Access*, vol. 6, pp. 66 020–66 029, 2018.

[16] D.-F. Guan, Q. Zhang, P. You, Z.-B. Yang, Y. Zhou, and S.-W. Yong, "Scanning rate enhancement of leaky-wave antennas using slow-wave substrate integrated waveguide structure," *IEEE Trans. Antennas Propag.*, vol. 66, no. 7, pp. 3747–3751, Jul. 2018.

[17] S.-D. Xu, D.-F. Guan, Q. Zhang, P. You, S. Ge, X.-X. Hou, Z.-B. Yang, and S.-W. Yong, "A wide-angle narrowband leaky-wave antenna based on substrate integrated waveguide-spoof surface plasmon polariton structure," *IEEE Antennas Wireless Propag. Lett.*, vol. 18, no. 7, pp. 1386–1389, Jul. 2019.

[18] J. Zhong, A. K. Rashid, and Q. Zhang, "45° linearly polarized and circularly polarized high-scanning-rate leaky-wave antennas based on slotted substrate integrated waveguide," *IEEE Access*, vol. 8, pp. 82 162–82 172, 2020.

[19] G. Zhang, Q. Zhang, Y. Chen, and R. D. Murch, "High-scanning-rate and wide-angle leaky-wave antennas based on glide-symmetry Goubau line," *IEEE Trans. Antennas Propag.*, vol. 68, no. 4, pp. 2531–2540, Apr. 2020.

[20] H. Jiang, K. Xu, Q. Zhang, Y. Yang, D. K. Karmokar, S. Chen, P. Zhao, G. Wang, and L. Peng, "Backward-to-forward wide-angle fast beam-scanning leaky-wave antenna with consistent gain," *IEEE Trans. Antennas Propag.*, vol. 69, no. 5, pp. 2987–2992, May 2021.

[21] H. Zhou, Y. Zhang, Q. Zhang, M. Yu, H. Wang, and R. D. Murch, "Design of coupled-resonator array antenna for steering beam with extremely high scanning rate," *IEEE Trans. Antennas Propag.*, vol. 70, no. 8, pp. 7228–7233, Aug. 2022.

[22] X. Fu, Z. Zhang, and J. Wang, "A compact frequency scanning planar array using characteristic mode analysis," *IEEE Antennas Wireless Propag. Lett.*, vol. 20, no. 9, pp. 1666–1670, Sept. 2021.

[23] Y. Zeng, D. Wu, J. Xiong, J. Liu, and D. Zhang, "MultiSense: Enabling multi-person respiration sensing with commodity WiFi," *Proc. ACM on Interact., Mobile, Wearable Ubiquitous Technol.*, pp. 47–56, Sept. 2020.

[24] S. Yue, H. He, H. Wang, H. S. Rahul, and D. Katabi, "Extracting multi-person respiration from entangled RF signals," *Proc. ACM Interact., Mobile, Wearable Ubiquitous Technol.*, pp. 1–22, Jul. 2018.

[25] X. Wang, C. Yanc, and S. Mao, "TensorBeat: Tensor decomposition for monitoring multi-person breathing beats with commodity WiFi," *ACM Trans. Intell. Syst. Technol.*, vol. 9, no. 1, pp. 1–27, Sep. 2017.

[26] C. Chen, Y. Han, Y. Chen, H.-Q. Lai, F. Zhang, B. Wang, and K. J. R. Liu, "TR-BREATH: Time-reversal breathing rate estimation and detection," *IEEE Trans. Biomed. Eng.*, vol. 65, no. 3, pp. 489–501, Mar. 2018.

[27] H. Wang, D. Zhang, J. Ma, Y. Wang, Y. Wang, D. Wu, T. Gu, and B. Xie, "Human respiration detection with commodity WiFi devices: Do user location and body orientation matter?" in *Proc. ACM Int. Joint Conf. Pervasive Ubiquitous Comput. (Ubicomp)*, 2016, pp. 25–36.

[28] F. Zhang, Z. Chang, K. Niu, J. Xiong, B. Jin, Q. Lv, and D. Zhang, "Exploring lora for long-range through-wall sensing," *Proc. ACM Interact., Mobile, Wearable Ubiquitous Technol.*, vol. 4, no. 2, pp. 1–27, Jun. 2020.

[29] F. Zhang, D. Zhang, J. Xiong, H. Wang, K. Niu, B. Jin, and Y. Wang, "From Fresnel diffraction model to fine-grained human respiration sensing with commodity Wi-Fi devices," *Proc. ACM Interact., Mobile, Wearable Ubiquitous Technol.*, vol. 2, no. 1, pp. 1–23, 2018.

[30] Y. Zeng, D. Wu, R. Gao, T. Gu, and D. Zhang, "FullBreathe: Full human respiration detection exploiting complementarity of CSI phase and amplitude of WiFi signals," *Proc. ACM Interact., Mobile, Wearable Ubiquitous Technol.*, vol. 2, no. 3, pp. 1–19, 2018.

[31] Y. Zeng, D. Wu, J. Xiong, E. Yi, R. Gao, and D. Zhang, "FarSense: Pushing the range limit of WiFi-based respiration sensing with CSI ratio of two antennas," *Proc. ACM Interact., Mobile, Wearable Ubiquitous Technol.*, vol. 3, no. 3, pp. 1–26, 2019.

[32] X. Wang, K. Niu, J. Xiong, B. Qian, Z. Yao, T. Lou, and D. Zhang, "Placement matters: Understanding the effects of device placement for WiFi sensing," *Proc. ACM Interact., Mobile, Wearable Ubiquitous Technol.*, vol. 6, no. 1, pp. 1–25, 2022.

[33] H. Hu and K.-L. Wu, "A generalized coupling matrix extraction technique for bandpass filters with uneven-Qs," *IEEE Trans. Microw. Theory Techn.*, vol. 62, no. 2, pp. 244–251, Feb. 2014.

[34] NeuLog Logger Sensors, Respiration Monitor Belt logger sensor NUL-236, [Online]. Available: https://neulog.com/respiration-monitor-belt/.

[35] F. Zhang, Z. Chang, J. Xiong, R. Zheng, and D. Zhang, "Unlocking the beamforming potential of LoRa for long-range multi-target respiration sensing," *Proc. ACM on Interact., Mobile, Wearable Ubiquitous Technol.*, pp. 1–25, 2021.

[36] Z. Chang, F. Zhang, J. Xiong, W. Chen, and D. Zhang, "MSense: Boosting wireless sensing capability under motion interference," *Proc. ACM MobiCom.*, 2024.